Bulletin of the Seismological Society of America, Vol. 96, No. 3, pp. 1003–1011, June 2006, doi: 10.1785/0120050129

Earthquake Relocation and Focal Mechanism Determination Using Waveform Cross Correlation, Nicoya Peninsula, Costa Rica

by Samantha E. Hansen, Susan Y. Schwartz, Heather R. DeShon, and Victor González

Abstract The Nicoya Peninsula in Costa Rica directly overlies the seismogenic zone of the Middle America Trench, making it an ideal location for geophysical investigations of shallow subduction zone earthquake processes. As part of the collaborative Costa Rica Seismogenic Zone Experiment (CRSEIZE), a seismic network consisting of 20 land and 14 ocean-bottom seismometers recorded small magnitude local earthquakes along the Nicoya Peninsula from December 1999 to June 2001. Previous studies have used these data to compute local earthquake locations and 3D velocity structure to identify plate boundary seismicity and to investigate seismogenic behavior. Here we utilize waveform cross-correlation and clustering techniques in an attempt to improve earthquake relocations and determine first-motion focal mechanisms to validate, refine, and expand on existing models. Due to the high quality of the original locations and the small cross-correlation *P*-wave arrival time adjustments, large differences between the previously determined and the cross-correlated earthquake locations are not observed. However, focal mechanism determinations using cross-correlated *P* waveforms are significantly enhanced. Approximately 90% of the focal mechanisms computed for events previously identified as interplate earthquakes are consistent with underthrusting. Focal mechanisms for continental intraplate events indicate dextral strike-slip motion in the central region and normal faulting at the southern tip of the peninsula. These motions may be associated with oblique convergence and seamount subduction, respectively. Within the subducting plate, steep *P* and *T* axes of earthquakes below 50 km depth are consistent with unbending of the slab.

Introduction

The properties controlling the up- and downdip limits of seismicity within seismogenic zones at convergent margins are poorly understood since most seismogenic zones begin far offshore and are therefore difficult to instrument. However, along western Costa Rica, the Nicoya Peninsula lies directly over the seismogenic zone of the Middle America Trench (MAT), making this region an ideal location for geophysical investigations. As part of the collaborative 1999–2001 Costa Rica Seismogenic Zone Experiment (CRSEIZE), an onshore–offshore seismic network consisting of both broadband and short-period three-component land and broadband three-component ocean-bottom seismometers was established along the Nicoya Peninsula (Fig. 1). The array recorded 18 months of local seismicity to gain a better understanding of plate boundary processes occurring at subduction environments.

Previous work in this area examined the effects of seafloor roughness and thermal history on the earthquake rupture process and on the loci of seismogenic zone seismicity (Newman *et al.*, 2002; Bilek *et al.*, 2003; DeShon *et al.*, 2003). Local seismic tomography was also applied to image the 3D *P*- and *S*-wave velocity structure in the vicinity of the seismogenic zone in northern Costa Rica and to identify events occurring along the plate interface (DeShon *et al.*, 2006). These studies illustrated that the width and depth extent of the seismogenic zone varies along strike of the MAT. Norabuena *et al.* (2004) modeled geodetic data, which was also collected as part of the CRSEIZE, and compared it to the distribution of interplate seismicity. It was found that the loci of microseismicity occurred between two patches of strong geodetic locking, in a region that appeared to be creeping at close to the plate rate. These types of observations emphasize the importance of accurately identifying and locating interplate seismicity in this region.

In this study, we use waveform cross-correlation techniques in an attempt to improve *P*-wave arrival times. The automated correlation and clustering method employed greatly reduces picking inconsistencies as compared to human analysis alone (Rowe *et al.*, 2002a). Cross correlation has shown great success in varied tectonic environments in-

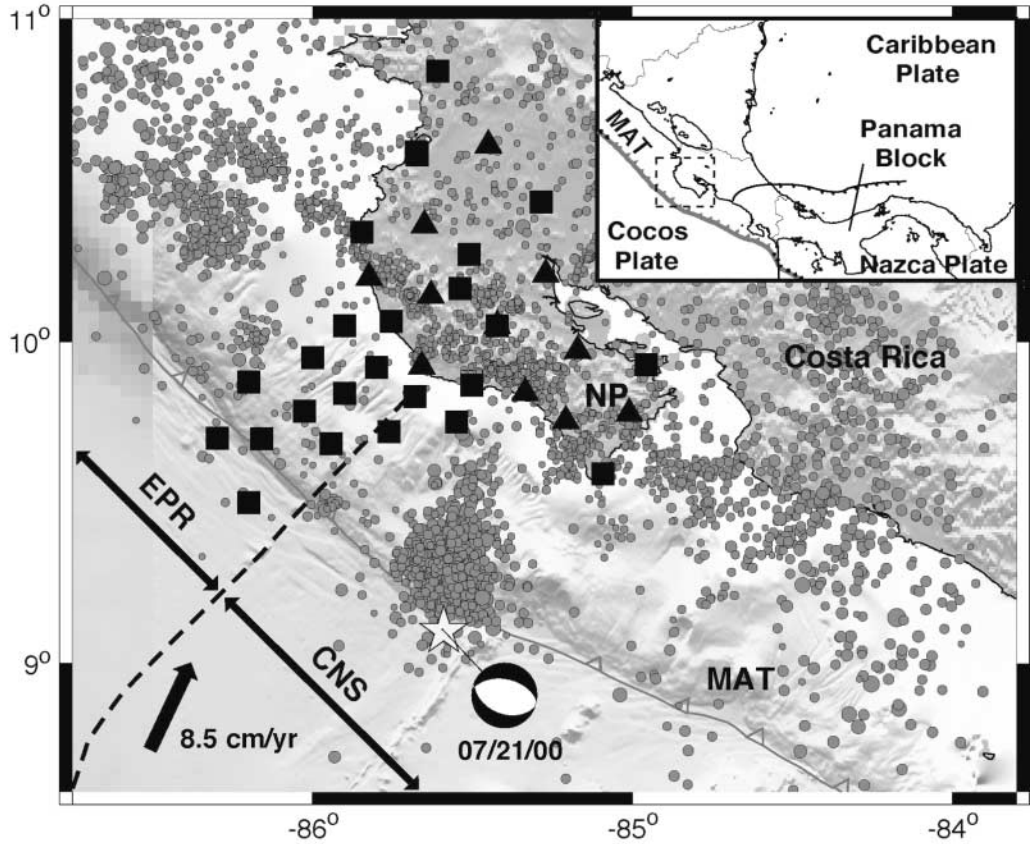

Figure 1. Overview map of the Nicoya CRSEIZE experiment. Cocos Plate oceanic crust formed at the East Pacific Rise (EPR) and at the Cocos-Nazca Spreading Center (CNS) subducts along the Middle America Trench (MAT) offshore northern Costa Rica. The EPR-CNS plate suture occurs along a triple junction trace (bold dashed line). The Nicoya experiment recorded interseismic interplate and crustal seismicity, including the mainshock and aftershock sequence of the 2000 Nicoya earthquake along the outer rise (star with Harvard Centroid Moment Tensor solution). Broadband stations are shown by squares, and short-period stations are shown by triangles. Initial database locations using 1D IASP91 velocity model are scaled by local magnitude (gray circles). NP: Nicoya Peninsula. Bathymetry is from von Huene *et al.* (2000).

cluding the Soultz Geothermal Reservoir (Rowe, Aster, Phillips, *et al.*, 2002), the Soufriere Hills volcano (Rowe *et al.*, 2004), the northern New Zealand subduction zone (Du *et al.*, 2004), and along sections of the Hayward, Calaveras, and San Andreas faults (Rubin, 2002; Waldhauser and Ellsworth, 2002). The goals of this study are to use cross-correlated waveforms to improve earthquake locations and determine reliable focal mechanisms. These results will validate, refine, and expand existing models to strengthen the conclusions of previous work, which examined interplate seismicity. The cross-correlated locations and focal mechanisms also provide additional constraints on intraplate seismicity, in both the overlying plate and in the subducting slab.

Tectonic Setting and Data

In northern Costa Rica, the oceanic Cocos plate subducts beneath the Caribbean plate at the MAT. Convergence is about 20° counterclockwise from trench normal at a rate of 83–85 mm/yr (Lundgren *et al.*, 1999; DeMets, 2001; Iinuma *et al.*, 2004; Norabuena *et al.*, 2004). The oceanic plate offshore northern Costa Rica originates from both the Cocos-Nazca Spreading Center (CNS) and the East Pacific Rise (EPR). While both types of lithosphere are of similar age at the MAT (20–25 Ma), there is a distinct thermal change across the EPR-CNS plate suture related to increased hydrothermal circulation in the upper 1–2 km of EPR-derived crust (Fisher *et al.*, 2003). Newman *et al.* (2002) and DeShon *et al.* (2006) imaged a 5- to 10-km offset in the updip limit of seismicity across the EPR-CNS plate boundary, which may be related to the thermal difference. The dip of the plate interface steepens along the Nicoya Peninsula from southeast to northwest and is consistent with regional trends (Protti *et al.*, 1995).

The Nicoya Peninsula seismic array recorded over 10,000 earthquakes (Fig. 1), and *P*- and *S*-wave arrival times

were picked for about 2000 local events (see Newman *et al.*, 2002, and DeShon *et al.*, 2006, for more details). Using the Nicoya Peninsula data set, DeShon *et al.* (2006) simultaneously inverted for hypocenters and 3D seismic velocities using both *P* and *S-P* travel times. The 611 events located using the simultaneous inversion (Fig. 2) are well constrained, with average error estimates of 0.58 km N, 0.60 km E, and 1.04 km depth and an average event root mean square residual of 0.14 sec (DeShon *et al.*, 2006). These events comprise the starting data set for waveform cross-correlation relocations and focal mechanism determinations.

While events in the overlying continental crust and events within the subducting slab are included, a majority of the 611 well-located earthquakes appear to occur along the plate interface, which was defined by DeShon *et al.* (2006) using previously published refraction data (Sallarès *et al.*, 2001) and 3D *P*-wave velocities. Events occurring from 5 km below to 8 km above the plate interface, down to a depth of 40 km, were identified as interplate seismicity (Fig. 2). Since the dip of the plate interface changes from southeast to northwest, there appears to be some scatter in the event distribution when the seismicity is projected onto a single plane perpendicular to the trench. This is highlighted by the offset in the EPR and CNS interplate seismicity in Figure 2. In general, interplate seismicity beneath the Nicoya Peninsula appears to cease just updip of the continental Moho/slab intersection, which occurs between 30 and 34 km depth (Sallarès *et al.*, 1999, 2001; DeShon and Schwartz, 2004; DeShon *et al.*, 2006). Refined relocations and focal mechanisms computed with the cross-correlated waveforms will allow interplate and intraplate events to be differentiated.

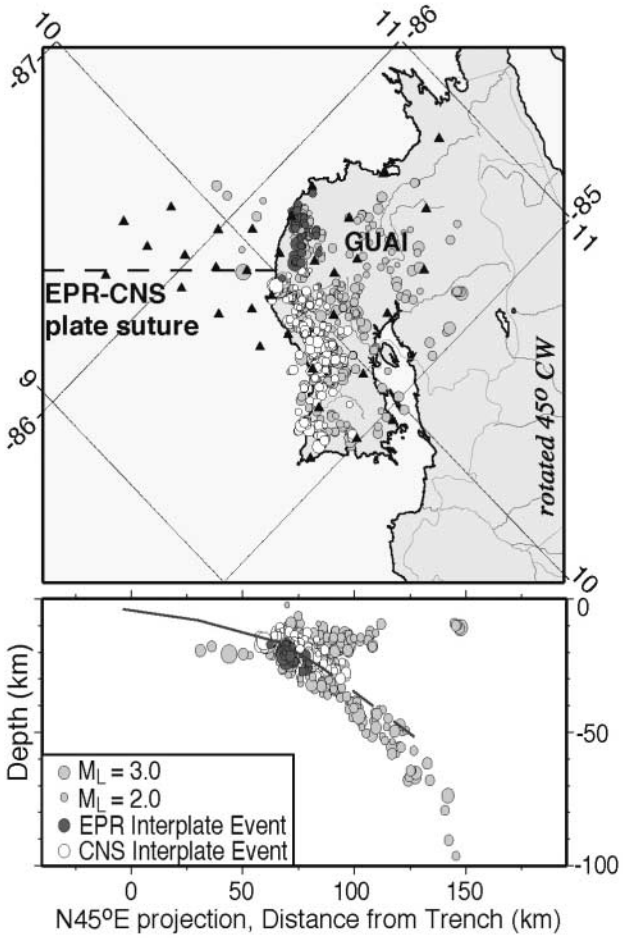

Figure 2. Map view and cross section showing the original locations obtained by DeShon *et al.* (2006). The dark gray and white circles highlight those events identified as EPR and CNS interplate seismicity, respectively. The light gray circles represent intraplate events. All events are scaled by their local magnitudes. The line in the cross section represents the interpreted plate interface. The trace of the EPR-CNS plate suture (dashed line) and the master station used for waveform cross correlation, GUAI, are also labeled.

Methodology

Waveform Cross Correlation

We employ an automatic cross-correlation and clustering algorithm developed by Rowe, Aster, Borchers, *et al.* (2002) to assess waveform similarity between events in the Nicoya data set. This method assumes that earthquakes that occur in close proximity will share similar source processes and event-receiver paths, yielding nearly identical waveforms. The events are first separated into related families based on cross-correlation coefficients at a master station using a dendritic clustering scheme. Subdivision of the data continues until a user-specified coefficient threshold is reached. The final clusters obtained depend on both the threshold and the window length used to correlate the waveforms (Rowe, Aster, Borchers, *et al.*, 2002).

For the Nicoya data set, the 611 well-located earthquakes from DeShon *et al.* (2006) were spatially grouped into 0.1° latitude by 0.1° longitude by 10-km-depth boxes to ensure event proximity. Then, within each spatial group, vertical component seismograms of each event were cross-correlated and clustered. Station GUAI (Fig. 2) was used as the master station because it had the most observations and generally displayed a higher signal-to-noise ratio than many of the other stations. Several different window lengths were tested, but because the *P*-wave onset is of primary interest, a relatively short window of 40 samples (1 sec) was selected (with one-quarter of the window before the *P*-wave arrival). To ensure maximum similarity between clustered events, a coefficient threshold of 0.90 was used at the master station. A total of 166 clusters were obtained, but over half of these clusters only contain event pairs or triplets. The small number of events per cluster may be due to the nature of the data set: the duration of the study was relatively short and the events are spread over a large volume. Given the small num-

ber of similar *P* waveforms, we did not attempt correlation of the noisier and sparser *S*-wave arrivals.

After the data have been divided into similar clusters based on waveform similarity at the master station, *P* waves within each group are cross-correlated at the remaining stations in the array. The methodology is the same as for the master station, however a smaller coefficient threshold of 0.80 was used to allow more leniency in the correlation of stations that have lower signal-to-noise ratios. Intracluster arrival time pick adjustments are solved for using an L_1-norm conjugate gradient method (Rowe, Aster, Borchers, *et al.*, 2002). This technique has been shown to significantly improve pick consistency as compared to analyst-defined picks. Figure 3 illustrates an example of adjusted picks for a cluster containing 5 earthquakes in the Nicoya data set. While the corrections to the *P*-wave picks do improve their consistency, it should be noted that most of the picks were not adjusted very much. Overall, the mean shift applied is about 2.20 samples, or about 0.06 sec for the land stations.

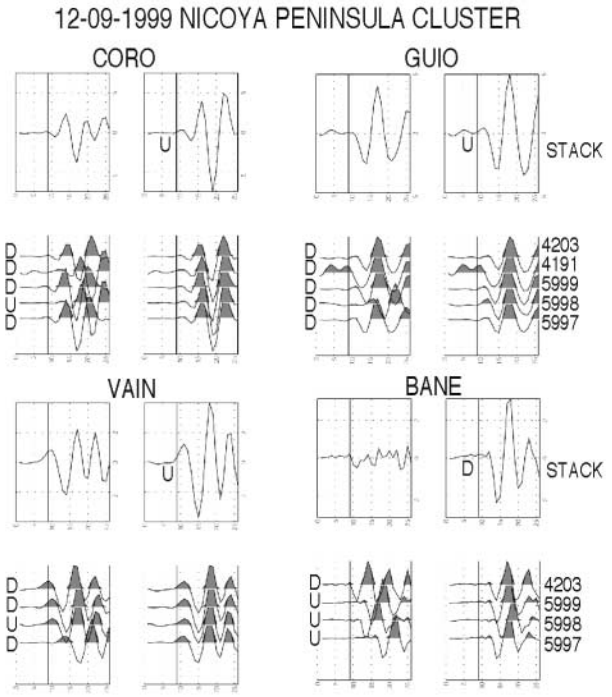

Figure 3. The panels show the waveforms at four different stations for a cluster of correlated events, all of which occurred on 9 December 1999. The panels on the left show the stacked (top) and individual (bottom) waveforms aligned on the original hand picks, while the panels on the right show the stacked (top) and individual (bottom) waveforms aligned on the cross-correlated picks. The U or D indicate up or down first motion, respectively, and the event numbers are listed along the right side.

Computing Relocations

The adjusted *P*-wave arrival time picks determined from cross correlation were used in an attempt to improve earthquake relocations using the algorithm hypoDD. HypoDD solves for the relative locations of events within closely spaced groups and uses ray tracing within a 1D velocity model to calculate travel-time differences (Waldhauser and Ellsworth, 2000). We use the minimum 1D velocity model resulting from simultaneous inversion of the Nicoya data set and a V_p/V_s ratio of 1.78, similar to the velocity ratio used in other central Costa Rica studies (Protti *et al.*, 1995; Quintero and Güendel, 2000; DeShon *et al.*, 2003; DeShon and Schwartz, 2004).

Correlated *P*-wave arrival times were substituted for analyst-defined *P*-wave picks where applicable. Since *S* waves were not correlated, the analyst-defined *S*-wave arrivals were used in all cases. However, the *S* waves were down-weighted 0.50 relative to the *P* waves to account for the increased reading error associated with this data. Using this approach, 496 of the original 611 events met the event separation criteria and were relocated. HypoDD does not solve for absolute earthquake locations; however, we are interested in how the overall pattern of seismicity changed using the more consistent pick times obtained from cross-correlation.

Computing Focal Mechanisms

Signal-to-noise ratios for the small-magnitude earthquakes occuring along the Nicoya Peninsula differ across the seismic array and complicate polarity identification. Focal mechanism solutions based on analyst-defined polarity picks vary significantly even for nearby events and are poorly constrained. Using an intracluster focal mechanism calculation approach leads to more consistent, reliable mechanisms as compared to those obtained from individual events. Cross-correlated vertical waveforms were used to compute *P*-wave first motion focal mechanisms for event clusters. This approach allows mechanisms for small events with fewer polarity observations to be determined by association with larger events in a cluster. For a given cluster, the first motion polarity at a selected station should be the same for all events since the waveforms are similar. Therefore, if data are not available for a small event at a given station, the first-motion polarity for that event can be extrapolated from the other events in the cluster. This not only improves the polarity pick consistency but also maximizes the number of polarity observations available to compute the corresponding focal mechanisms.

Focal mechanism determinations were attempted for all clustered events and for individual events with magnitudes $\geq$3.0 or that were believed to occur on the plate boundary. First-motion polarities were determined through visual inspection of the *P*-wave arrivals, and the distances and take-off angles were computed with the HypoInverse2000 algorithm (Klein, 2000) using fixed event locations and the same velocity model used in hypoDD. Focal mechanisms were then computed using FPFIT, which solves for double-couple

fault plane solutions using a grid search method (Reasenberg and Oppenheimer, 1985). For the clustered events, the polarity observations and an averaged hypocenter location for each group were used to generate a composite focal mechanism. For individual events, it was required that at least seven high-quality polarity observations distributed over a 130° azimuthal range were available. The combined results allow for a more complete characterization of the stress conditions in the vicinity of the seismogenic zone.

Discussion of Results

Cross-Correlated Event Relocations

Of the 496 events that were relocated using the cross-correlated arrival times, 33 events had position changes that were less than the average error estimates for the original locations. Therefore, these 33 events are assumed to have unchanged or "fixed" positions and are used to place the relative cross-correlation relocations with respect to the absolute locations obtained by DeShon *et al.* (2006). On a regional scale, the cross-correlated relocations are somewhat improved, though not dramatically different, from the simultaneous inversion locations (Fig. 4a). The change in relocations is more apparent when viewed on a smaller scale, such as within a cluster of similar earthquakes (Fig. 4b). In the provided example, the relocations within the cluster changed by up to 2 km. Overall, the difference in the weighted root mean square residual between the initial and final locations is 0.11 sec, corresponding to a data variance reduction of about 22%.

Most of the arrival-time adjustments applied to the correlated waveforms were relatively small, averaging about 2.20 samples (0.06 sec). It is believed that since the *P* waves were only adjusted a small amount and since low-error event locations were used to begin with, the use of cross-correlated picks did not lead to large-scale differences. In addition, since *S* waves were not correlated and analyst-picks were used for those arrivals, they may contribute to the small relocation changes obtained as well, even though the *S* waves were not weighted as highly in the hypoDD inversion. These results validate the previously determined locations, supporting the conclusions of Norabuena *et al.* (2004) and DeShon *et al.* (2006), whose interpretations were based on the distribution of seismicity.

Focal Mechanisms for Interplate Seismicity

Focal mechanisms were computed for both clusters and individual events that appear to occur on the plate boundary. Figure 5 shows a map view of all the cross-correlated relocations, highlighting those events identified by DeShon *et al.* (2006) as occurring on the plate boundary, with the computed focal mechanisms. Figure 6 displays the same data as Figure 5 in cross section. The examined events span almost the entire along-dip length of the seismogenic zone, providing a thorough representation of the stress conditions along the plate interface.

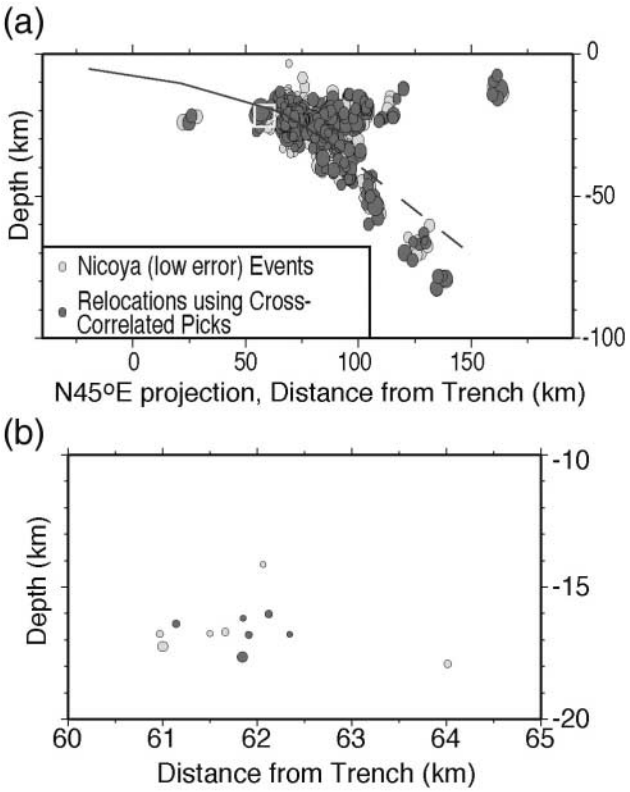

Figure 4. Comparison of locations from 3D inversion and waveform cross correlation. (a) Cross section showing the original locations from DeShon *et al.* (2006, light gray circles) and the revised locations using cross-correlated picks (dark gray circles). On a regional scale, the locations are very similar. The small box indicates the location of one of the correlated clusters. (b) The cluster highlighted by the small box in (a). On this smaller scale (within the cluster) the changes in locations between the original (light gray circles) and the revised locations obtained from cross correlation (dark gray circles) are more apparent. Note how the cross-correlated relocations are more tightly grouped, forming a more cohesive cluster.

Approximately 90% of the computed mechanisms are consistent with underthrusting. Some of the focal mechanisms shown have been slightly adjusted without violating any of their first-motion picks to fit the expected thrust orientation. Therefore, it is estimated that the reported strike, dip, and rake values are accurate to within about 15°. The change of the plate interface dip across the EPR-CNS plate suture is clearly observed in Figure 6, where two distinct layers of underthrusting are imaged. These results confirm the offset in the seismicity associated with the subducting EPR and CNS lithospheres and the interpretation based on spatial proximity that these earthquakes are occurring along the plate boundary (Newman *et al.*, 2002; DeShon *et al.*, 2006). The uncertainty of up to 15° in nodal plane dip makes

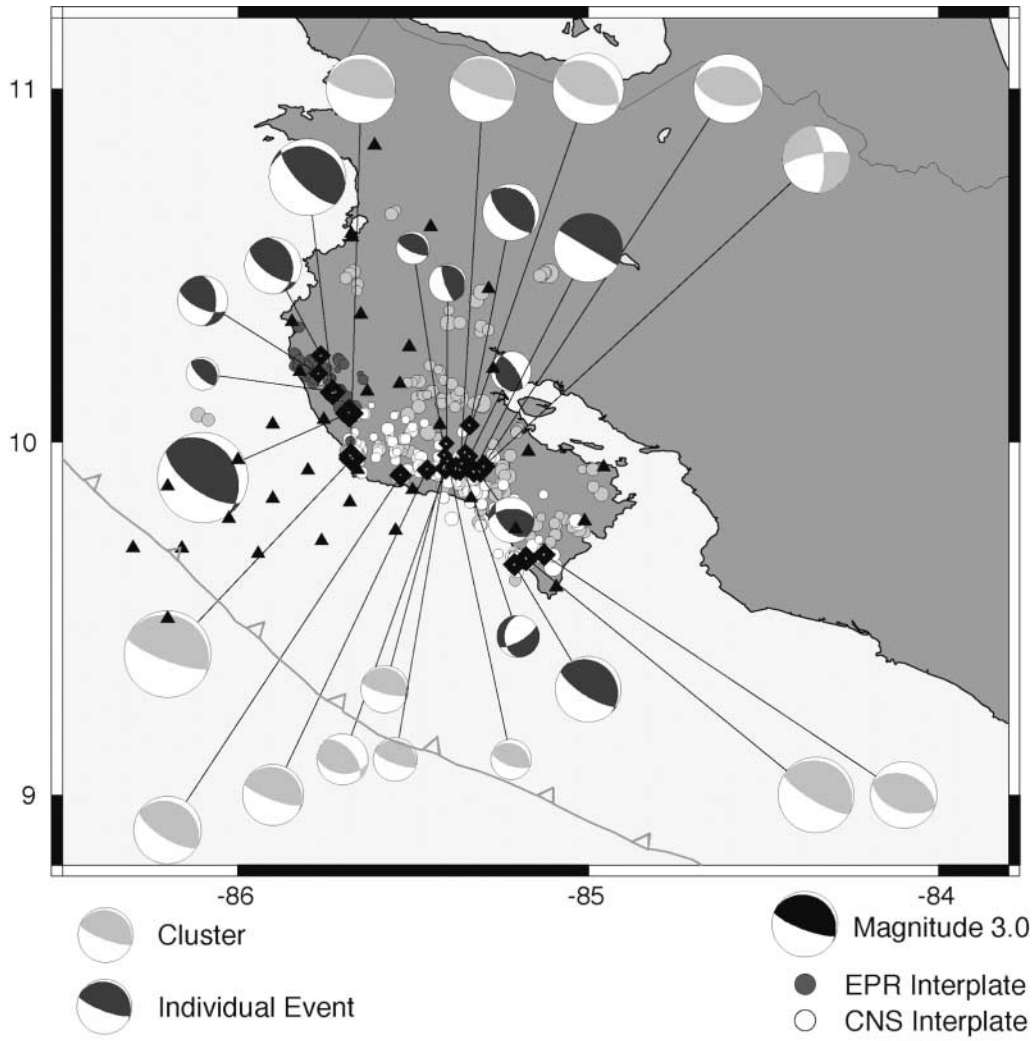

Figure 5. Focal mechanisms for previously assumed (DeShon *et al.*, 2006) interplate seismicity. Map showing all cross-correlated relocations (light gray circles), highlighting the events identified as EPR and CNS interplate seismicity by DeShon *et al.* (2006) (dark gray and white circles, respectively). Interplate events for which focal mechanisms could be computed are marked by black diamonds, and the corresponding mechanisms are shown. The focal mechanisms were computed for both clusters of correlated events (lighter beach balls) and individual events (darker beach balls). Both the seismicity and the focal mechanisms are scaled by magnitude. For clustered events, the average location and mechanism is shown.

this change in plate interface dip impossible to detect in the focal mechanism determinations.

Focal Mechanisms for Intraplate Seismicity

In addition to the interplate events examined, focal mechanisms were computed for a number of magnitude $\geq$3.0 earthquakes in the overlying continental crust and in the subducting slab. However, it should be noted that some of these events were not relocated during the simultaneous inversion for location and velocity structure because they did not meet standard quality criteria (DeShon *et al.*, 2006). Therefore, the hypocenters of these events are not as well constrained as the events that were relocated. Yet, the focal mechanisms obtained can still provide insight into the stress conditions within the overriding and subducting plates.

In the overlying crust, two distinct types of focal mechanisms are observed (Fig. 7a). In the central part of the peninsula, a cluster of five relocated and cross-correlated events display nearly pure strike-slip motion. We favor the northwest-striking nodal plane and interpret right-lateral motion on this plane as accommodating the trench-parallel component of the slip vector. As mentioned previously, the convergence at the MAT is oblique, approximately 20° counterclockwise from trench normal (Lundgren *et al.*, 1999; Iinuma *et al.*, 2004; Norabuena *et al.*, 2004). Norabuena *et*

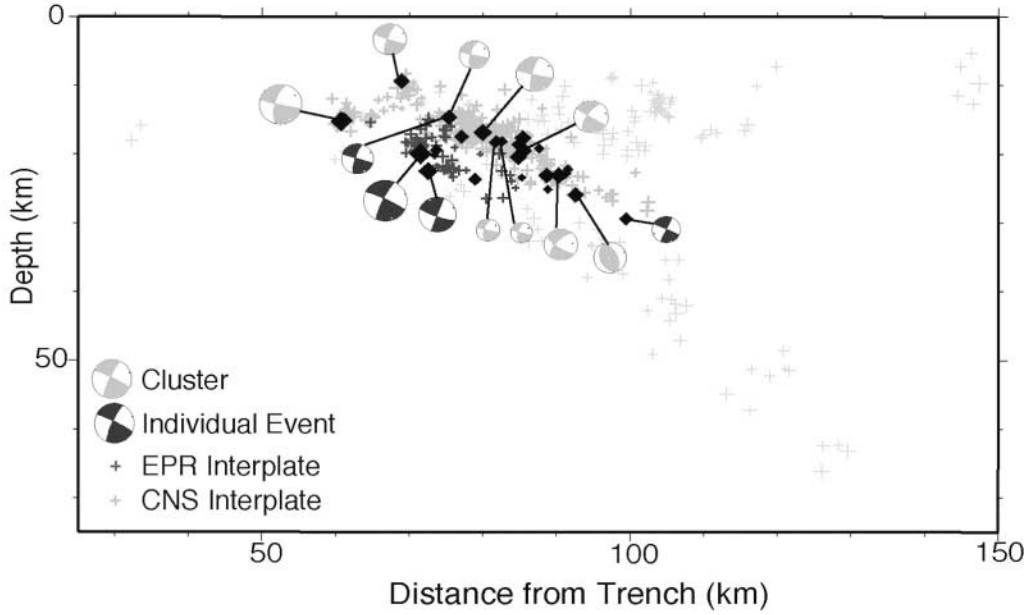

Figure 6. Interplate focal mechanisms in cross section. The thick light gray and dark gray crosses highlight the events identified as CNS and EPR interplate seismicity by DeShon *et al.* (2006), respectively. Interplate events for which focal mechanisms could be computed are marked by black diamonds, and selected focal mechanisms from Figure 5 are shown. Again, focal mechanisms were computed for both correlated events (lighter beach balls) and individual events (darker beach balls). The examined events span almost the entire length of the seismogenic zone, and a significant percentage are consistent with underthrusting.

al. (2004) demonstrated that 8 ± 3 mm/yr of northwest forearc motion is required to fit the geodetic observations in this area. The computed mechanisms are consistent with this type of slip partitioning, although the preferred fault plane strikes approximately 25° more northerly than the trench. Several historical events in this region, such as the 1973 Tilaran earthquake, some 50 km landward from this cluster, also displayed right-lateral strike-slip motion on northwest-striking fault planes (Güendel, 1986). While structures that might accommodate this type of motion are not clear along the Nicoya Peninsula, these events may be associated with the Rio Morote fault described by Dengo (1962).

At the southern tip of the Nicoya Peninsula, two individual events display similar focal mechanisms that indicate extension in the overlying crust (Fig. 7a). The locations of these two events are not as well constrained, but it appears that at least one of these events is fairly close to the plate boundary (Fig. 7b). Several previous studies have shown that the Fischer seamount group is subducting beneath the end of the Nicoya Peninsula, causing deformation and uplift in the continental crust (Dominguez *et al.*, 1998; Fisher *et al.*, 1998; Ranero and von Huene, 2000; Gardner *et al.*, 2001). Normal faults, either directly above or in the wake of the seamount, exhibit extension similar to that observed here (Dominguez *et al.*, 1998; Ranero and von Huene, 2000). Therefore, these mechanisms may reflect some of the effects seafloor roughness has on fault kinematics.

A number of intraplate events in the subducting slab were also examined, most of which occurred below a depth of 50 km (Fig. 7b). The locations and orientations of these events are not as well constrained as the other events in this study; however, some interesting observations can still be made. It appears that the focal mechanisms for the shallower events in this group display down-dip compression with *P* axes that dip steeply in the direction of subduction. However, the deeper events in this group display downdip tension. This variation may reflect unbending of the slab at depth. Protti-Quesada (1991) reported similar findings, with changes from vertical and subvertical compression to vertical and subvertical extension between depths of 50 and 75 km. Comparable observations have also been made at other subduction environments including northeastern Japan (Kosuga *et al.*, 1996; Christova and Tsapanos, 2000) and Kamchatka (Christova, 2001).

Conclusions

Waveform cross-correlation and clustering techniques were employed to assess the similarity of events in the CRSEIZE Nicoya dataset, and this similarity was exploited to improve earthquake location and focal mechanism determinations. The *P*-wave arrival-time adjustments obtained from cross correlation were small, providing only a limited improvement in earthquake location compared to the pre-

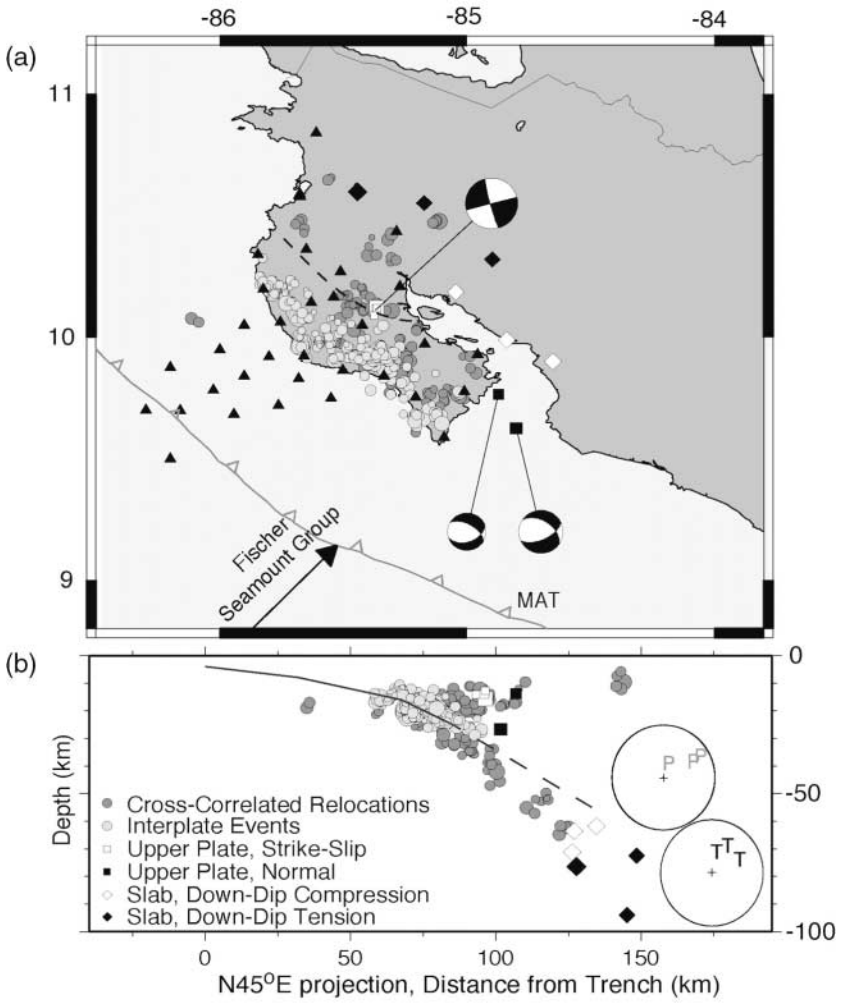

Figure 7. Map view (a) and cross section (b) highlighting the examined intraplate events. The upper plate earthquakes consist of a correlated cluster of five events displaying dextral strike-slip motion (white squares) and two events displaying normal motion (black squares). These may be associated with oblique convergence and seamount subduction, respectively. The dashed line on the peninsula (a) marks the approximate location of the Rio Morote fault, and the arrow offshore shows the trend of the subducting Fischer seamount group. In the subducting slab, the shallower examined events (white diamonds) all have steep *P* axes and are consistent with downdip compression. However, the deeper events (black diamonds) all have steep *T* axes and are consistent with downdip tension. This may reflect unbending of the slab at depth.

viously obtained locations (DeShon *et al.*, 2006). Focal mechanism determinations using the cross-correlated picks were significantly enhanced, as correlated clusters are useful in aiding the analyst to define first-motion polarity. For those events previously identified as interplate seismicity, focal mechanism determinations revealed that about 90% of the events analyzed are consistent with underthrusting. Focal mechanisms computed for intraplate events in the overlying and subducting plates also provided constraints on the stress conditions in these areas. In the overlying plate, evidence for both dextral strike-slip and normal motion is seen along the peninsula. These motions may be associated with oblique convergence and seamount subduction, respectively. In the subducting plate, the *P* and *T* axes of events at depth are consistent with unbending of the slab.

Acknowledgments

We would like to thank Marino Protti, Dan Sampson, Andy Newman, and Sue Bilek for their assistance with the deployment and operation of the land instruments, LeRoy Dorman, Alan Sauter, Sharon Escher, and GEOMAR for their assistance with OBS deployment, data processing, and recovery, and Marino Protti and Stephan Husen for their careful reviews of this manuscript, which improved its content. Some of the instruments used were provided by the PASSCAL Instrument Center at New Mexico Tech. In addition, we would like to thank Charlotte Rowe for her help with the waveform cross-correlation study. Figures were made using GMT (Wessel and Smith, 1998). Funding for this project was partially provided by National Science Foundation Grant No. EAR0229876, awarded to S. Y. Schwartz.

References

Bilek, S. L., S. Y. Schwartz, and H. R. DeShon (2003). Control of seafloor roughness on earthquake rupture behavior, *Geology* **31,** 455–458.

Christova, C. (2001). Depth distribution of stresses in the Kamchatka Wadati-Benioff zone inferred by inversion of earthquake focal mechanisms, *J. Geodynam.* **31,** 355–372.

Christova, C., and T. Tsapanos (2000). Depth distribution of stresses in the Hokkaido Wadati-Benioff zone as deduced by inversion of earthquake focal mechanisms, *J. Geodynam.* **30,** 557–573.

DeMets, C. (2001). A new estimate for present-day Cocos-Caribbean plate motion: implications for slip along the Central American volcanic arc, *Geophys. Res. Letts.* **28,** 4043–4046.

Dengo, G. (1962). Geologic map of the Province of Guanacaste and adjacent zones, Instituto Geografico de Costa Rica, scale 1:300,000.

DeShon, H. R., and S. Y. Schwartz (2004). Evidence for serpentinization of the forearc mantle wedge along the Nicoya Peninsula, Costa Rica, *Geophys. Res. Letts.* **31,** L21611, doi 10.1029/2004GL021179.

DeShon, H. R., S. Y. Schwartz, S. L. Bilek, L. M. Dorman, V. Gonzalez, J. M. Protti, E. R. Flueh, and T. H. Dixon (2003). Seismogenic zone structure of the southern Middle America Trench, Costa Rica, *J. Geophys. Res.* **108,** 2491, doi 10.1029/2002JB002294.

DeShon, H. R., S. Y. Schwartz, A. V. Newman, V. González, M. Protti, L. M. Dorman, T. H. Dixon, E. O. Norabuena, and E. R. Flueh (2006). Seismogenic zone structure beneath the Nicoya Peninsula, Costa Rica, from 3D local earthquake *P*- and *S*-wave tomography, *Geophys. J. Int.* **164,** 109–124.

Dominguez, S., S. E. Lallemand, J. Malavieille, and R. von Huene (1998). Upper plate deformation associated with seamount subduction, *Tectonophysics* **293,** 207–224.

Du, W., C. H. Thurber, M. Reyners, D. Eberhart-Phillips, and H. Zhang (2004). New constraints on seismicity in the Wellington region of New Zealand from relocated earthquake hypocenters, *Geophys. J. Int.* **158,** 1088–1102.

Fisher, A. T., C. A. Stein, R. N. Harris, K. Wang, E. A. Silver, M. Pfender, M. Hutnak, A. Cherkaoui, R. Bodzin, and H. Villinger (2003). Abrupt thermal transition reveals hydrothermal boundary and role of seamounts within the Cocos Plate, *Geophys. Res. Letts.* **30,** 1550, doi 10.1039/2002GL016766.

Fisher, D. M, T. W. Gardner, J. S. Marshall, P. B. Sak, and M. Protti (1998). Effect of subducting sea-floor roughness on fore-arc kinematics, Pacific coast, Costa Rica, *Geology* **26,** 467–470.

Gardner, T., J. Marshall, D. Merritts, B. Bee, R. Burgette, E. Burton, J. Cooke, N. Kehrwald, M. Protti, D. Fisher, and P. Sak (2001). Holocene forearc block rotation in response to seamount subduction, southeastern Península de Nicoya, Costa Rica, *Geology* **29,** 151–154.

Güendel, F. (1986). Seismotectonics of Costa Rica: an analytical view of the southern terminus of the Middle America Trench, *Ph.D. Thesis*, University of California at Santa Cruz.

Iinuma, T., M. Protti, K. Obana, V. Gonzalez, R. van der Laat, T. Kato, S. Miyasaki, Y. Kaneda, and E. Hernandez (2004). Inter-plate coupling in the Nicoya Peninsula, Costa Rica, as deduced from a trans-peninsula GPS experiment, *Earth Planet. Sci. Letts.* 203–212.

Klein, F. W. (2000). User's guide to HYPOINVERSE-2000, a FORTRAN program to solve for earthquake locations and magnitudes, *U.S. Geol. Surv. Open-File Rep. 02-171*.

Kosuga, M., T. Sato, A. Hasegawa, T. Matsuzawa, S. Suzuki, and Y. Motoya (1996). Spatial distribution of intermediate-depth earthquakes with horizontal and vertical nodal planes beneath northeastern Japan, *Phys. Earth Planet. Inter.* **93,** 63–89.

Lundgren, P., M. Protti, A. Donnellan, M. Heflin, E. Hernandez, and D. Jefferson (1999). Seismic cycle and plate margin deformation in Costa Rica; GPS observations from 1994 to 1997, *J. Geophys. Res.* **104,** no. 12, 28,915–28,926.

Newman, A. V., S. Y. Schwartz, V. Gonzales, H. R. DeShon, J. M. Protti, and L. Dorman (2002). Along strike variability in the seismogenic zone below Nicoya Peninsula, Costa Rica, *Geophys. Res. Letts.* **29,** doi 10.1029/2002GL015409.

Norabuena, E., T. H. Dixon, S. Schwartz, H. DeShon, A. Newman, M. Protti, V. Gonzalez, L. Dorman, E. R. Flueh, P. Lundgren, F. Pollitz, and D. Sampson (2004). Geodetic and seismic constraints on some seismogenic zone processes in Costa Rica, *J. Geophys. Res.* **109,** doi 10.1029/2003JB002931.

Protti, M., K. McNally, J. Pacheco, V. Gonzalez, C. Montero, J. Segura, J. Brenes, V. Barboza, E. Malavassi, F. Güendel, G. Simila, D. Rojas, A. A. Velasco, A. Mata, and W. Schillinger (1995). The March 25, 1990 (M_w = 7.0, M_L = 6.8), earthquake at the entrace of the Nicoya Gulf, Costa Rica: its prior activity, foreshocks, aftershocks, and triggered seismicity, *J. Geophys. Res.* **100,** 20,345–20,358.

Protti-Quesada, J. M. (1991). Correlation between the age of the subducting Cocos plate and the geometry of the Wadati-Benioff zone under Nicaragua and Costa Rica, *M.S. Thesis*, University of California at Santa Cruz.

Quintero, R., and F. Güendel (2000). Stress field in Costa Rica, Central America, *J. Seism.* **4,** 297–319.

Ranero, C. R., and R. von Huene (2000). Subduction erosion along the Middle America convergent margin, *Nature* **404,** 748–752.

Reasenberg, P., and D. H. Oppenheimer (1985). FPFIT, FPPLOT, and FPPAGE, FORTRAN computer programs for calculating and displaying earthquake fault-plane solutions, *U.S. Geol. Surv. Open-File Rep. 85-739*, 109.

Rowe, C. A., R. C. Aster, B. Borchers, and C. J. Young (2002). An automatic, adaptive algorithm for refining phase picks in large seismic data sets, *Bull. Seism. Soc. Am.* **92,** 1660–1674.

Rowe, C. A., R. C. Aster, W. S. Phillips, R. H. Jones, B. Borchers, and M. C. Fehler (2002). Using automated, high-precision repicking to improve delineation of microseismic structures at the Soultz Geothermal Reservoir, *Pure Appl. Geophys.* **159,** 563–596.

Rowe, C. A., C. H. Thurber, and R. A. White (2004). Dome growth behavior at Soufriere Hills Volcano, Montserrat, revealed by relocation of volcanic event swarms, 1995–1996, *J. Volcan. Geotherm. Res.* **134,** 199–221.

Rubin, A. M. (2002). Using repeating earthquakes to correct high-precision earthquake catalogs for time-dependent station delays, *Bull. Seism. Soc. Am.* **92,** 1647–1659.

Sallarès, V., J. J. Dañobeitia, and E. R. Flueh (2001). Lithospheric structure of the Costa Rican isthmus: effects of subduction zone magmatism on an oceanic plateau, *J. Geophys. Res.* **106,** 621–643.

Sallarès, V., J. J. Dañobeitia, E. R. Flueh, and G. Leandro (1999). Seismic velocity structure across the middle American landbridge in northern Costa Rica, *J. Geodynam.* **27,** 327–344.

von Huene, R., C. R. Ranero, W. Weinrebe, and K. Hinz (2000). Quaternary convergent margin tectonics of Costa Rica: segmentation of the Cocos plate and Central American volcanism, *Tectonics* **19,** 314–334.

Waldhauser, F., and W. L. Ellsworth (2000). A double-difference earthquake location algorithm: method and application to the northern Hayward fault, California, *Bull. Seism. Soc. Am.* **90,** 1353–1368.

Waldhauser, F., and W. L. Ellsworth (2002). Fault structure and mechanics of the Hayward fault, California, from double-difference earthquake locations, *J. Geophys. Res.* **107,** doi 10.1029/2000JB000084.

Wessel, P., and W. Smith (1998). New, improved version of Generic Mapping Tools released, *Trans. Am. Geophys. Union (EOS)* **79,** 579.

University of California, Santa Cruz
Earth Sciences Department
1156 High Street
Santa Cruz, California 95064
shansen@es.ucsc.edu
susan@es.ucsc.edu
(S.E.H, S.Y.S.)

University of Wisconsin, Madison
Geology and Geophysics Department
Weeks Hall, 1215 Dayton Street
Madison, Wisconsin 53706
hdeshon@geology.wisc.edu
(H.R.D.)

Observatorio Vulcanológico y Sismológico de Costa Rica
Universidad Nacional
Apartado Postal: 2346-3000
Heredia, Costa Rica
vgonzale@una.ac.cr
(V.G.)

Manuscript received 23 June 2005.